

Effect of solvents on structural anisotropy of polyaniline thin films^{*}

Maciej Śniechowski^{1), **}, Tomasz Kozik¹⁾, Wojciech Łużny¹⁾

DOI: [dx.doi.org/10.14314/polimery.2017.855](https://doi.org/10.14314/polimery.2017.855)

Abstract: X-ray surface diffraction experiments performed on polyaniline/camphorsulfonic acid (PANI/CSA) thin films reveal high anisotropy of the five main crystalline peaks. This anisotropy is different for samples cast from *m*-cresol and cast from trifluoroacetic acid (TFA). Taking advantage of a recently published crystalline unit cell model, intensity distribution maps are calculated for these two types of samples. The anisotropy is in agreement with experiment, further validating the PANI/CSA model and showing that solvent molecules are not present in the unit cell.

Keywords: polyaniline, surface diffraction, simulations, film anisotropy, solvent.

Wpływ rozpuszczalnika na anizotropię cienkich warstw polianiliny

Streszczenie: Cienkowarstwowe, wykazujące silną anizotropię próbki polianilina/kwas kamforosulfonowy (PANI/CSA) zbadano metodą dyfrakcji powierzchniowej promieniowania rentgenowskiego. Wyniki pomiarów w geometriach: transmisyjnej, odbiciowej i pośrednich wykazały różnice między natężeniami pięciu głównych maksimów krystalicznych. Anizotropia próbek była różna w wypadku użycia różnych rozpuszczalników (*m*-cresol, kwas trifluorooctowy). Niedawno opublikowany model struktury PANI/CSA wykorzystano do obliczenia map natężeń, a następnie do porównań z wynikami pomiarów. Proponowany model poprawnie opisuje uporządkowanie w próbkach folii z PANI/CSA wylanych z różnych rozpuszczalników, bez konieczności uwzględniania w nim cząsteczek rozpuszczalnika. Świadczy to o tym, że cząsteczki rozpuszczalnika nie występują w strukturze PANI/CSA jako składniki komórki elementarnej.

Słowa kluczowe: polianilina, dyfrakcja powierzchniowa, symulacje, anizotropia cienkich warstw, rozpuszczalnik.

Despite being a well known polymer system studied for over twenty years, the exact structure of PANI/CSA remained unknown throughout this time span. Samples of this conducting [1] polymer system are obtained by protonating a polyaniline (abbr. PANI) base with camphorsulfonic acid (abbr. CSA). This compound remains a research subject, especially in the context of synthesis methods [2] and applications [3, 4].

One of the more interesting structural problems was the high anisotropy of PANI/CSA thin films, very clearly observed in synchrotron radiation grazing incident beam X-ray diffraction experiments reported in [5, 6]. Of the

five main crystalline peaks observed for this system, almost all have a distinct anisotropy.

A recent study taking advantage of molecular dynamics simulations [7, 8] revealed that a system of alternating double layers of PANI chains and CSA counter ions is a stable, highly ordered molecular architecture, which may be considered a new model of the structure of the crystalline regions of this polymer compound. These papers were followed by a report on a neutron diffraction study of this system [9], in which artificial intelligence algorithms were used to find a tentative model of a crystalline unit cell for those regions. This model allows performing calculations which are in agreement with neutron diffraction experiments. A schematic of the alternating bilayer structure found by the optimizer is shown in Fig. 1.

The aim of this paper is to elaborate on the results originally published in [6] and to use the model of the PANI/CSA crystalline unit cell from [9] for calculating two dimensional X-ray surface diffraction intensity maps. An agreement between intensity maps obtained from calculations and from an appropriate processing of the graz-

¹⁾ AGH University of Science and Technology, Faculty of Physics and Applied Computer Science, al. Adama Mickiewicza 30, 30-059 Krakow, Poland.

^{*}) Material contained in this article was presented at the X International Conference "X-Ray investigations of polymer structure", Ustroń, Poland, 6–9 December 2016.

^{**}) Author for correspondence; e-mail: Maciej.Sniechowski@fis.agh.edu.pl

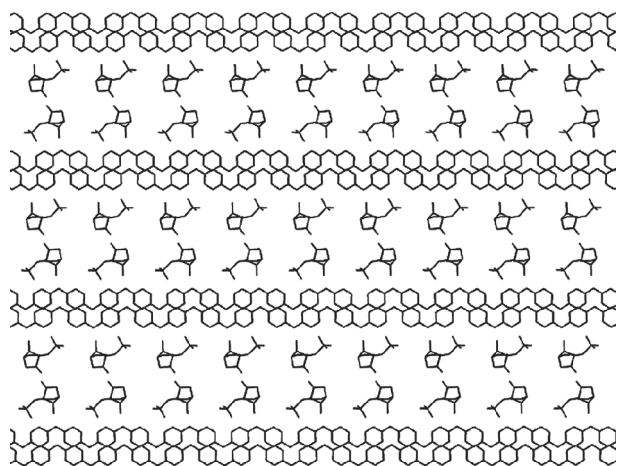


Fig. 1. Schematic of the alternating bilayer structure of the crystalline areas of the PANI/CSA conducting polymer system, as found by the optimizer; view perpendicular to unit cell b axis; unit cell c axis is parallel to polymer chains

ing data would strongly support the claim that this new model of the crystalline unit cell is in agreement with anisotropy investigations, which was originally made in [8] basing on an explanation of the possible orientations of the found structure versus the sample plane and then repeated in [9] basing on the Miller indexing of crystalline peaks calculated from the model.

EXPERIMENTAL PART

Materials and methods

Grazing incident beam measurements

The grazing incident beam measurements originally described in [5, 6] were performed using synchrotron radiation with a wavelength of 1.37 \AA , with the incident angle α smaller than 1° in all cases. Experimental data has the form of so-called radial scans. A single such scan is a record of scattered intensities measured at different detector positions. The position of the detector is given by the values of two angles γ and δ , the first of which is the angle between the outgoing beam and the sample surface, and the second between the outgoing beam and

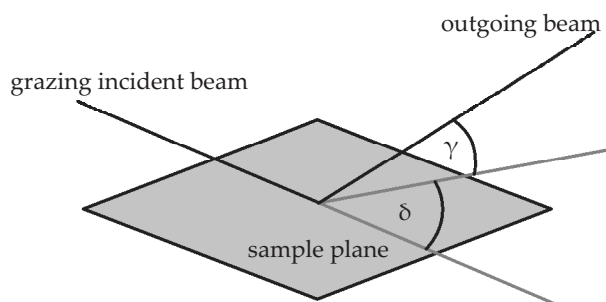


Fig. 2. Schematic depicting the physical meaning of the detector angles γ and δ

plane perpendicular to the sample plane, containing the incident beam. They are schematically depicted in Fig. 2.

In a radial scan either one of these angles is fixed, or the value of one is a linear function of the value of the other – radial scans are straight lines on the (δ, γ) plane. It is worth underlining that for values of δ close to 0 the experimental geometry corresponds to reflection geometry, and for values of γ close to 0 corresponds to transmission geometry. Hence the grazing incident beam technique allows investigating the anisotropy of thin samples by performing measurements in both of these geometries and all intermediate ones.

Two different thin film PANI/CSA samples were measured using this technique. They differed in the type of solvent used in the process of casting them. For the first one, the solvent was *m*-cresol, while for the other trifluoroacetic acid (abbr. TFA) was used. Very interestingly, the two samples exhibit almost opposite anisotropy, except the second peak, which is always oriented in the q_{xy} direction. For the first sample 9 radial scans were available, and for the other only 5.

Experimental data processing

Raw experimental data after applying aerial correction cannot be directly used in this study due to several reasons.

Firstly, the measured intensities are sums of the background, amorphous, and crystalline components, while calculations for a model crystalline unit cell only allow reproducing the crystalline component. Thus, the data must be processed by an algorithm subtracting the two unneeded components. In the case of each radial scan, processed separately, the input data is very slightly smoothed to reduce the noise. Then, the background and slope of the incident beam (registered at small angles) is subtracted. Next, a curve representing the amorphous component is calculated by copying the processed curve and performing 10 smoothing steps on it using an averaging smoothing algorithm with the radius of 15 data points, with the imposed rule that a single step cannot increase the intensity of a data point. Apart from the last two smoothing passes, the highest intensity of the calculated amorphous curve is not allowed to drop below 1.6 times the average intensity of the curve obtained after background and incident beam slope subtraction. If the algorithm attempts to do this, the intensity at maximum and 10 neighboring points on each side is set to the mean value. This guarantees that no negative intensity value will be produced by the procedure and also enables obtaining a Lorentzian-like curve. Such a calculated curve approximating the amorphous component is subtracted from the previous curve, which gives as a result a fairly good estimation of the crystalline component. This algorithm was found to perform well for all of the recorded scans, despite the significant differences between them.

Secondly, the data points are given in the (δ, γ) domain, while calculations will be giving data points in a (q_x, q_y, q_z)

domain, where q_{xy} denotes the length of the scattering vector projected onto the sample plane and q_z the length of its component in the direction perpendicular to the sample plane. The transformation from (δ, γ) to (q_{xy}, q_z) is straightforward and unambiguous and the data points were processed in this way.

Lastly, the calculation results cover all geometrically possible points of the (q_{xy}, q_z) plane, while in the experiment this plane was very sparsely probed. The underlying technical issue was that a CCD camera was unavailable at that time and thus only the earlier described radial scans could be recorded (although on the other hand, extracting the background and amorphous components could be more difficult in the other case). Therefore an interpolation algorithm is used to obtain a full two dimensional map from the processed experimental data. Such a map allows a better visual comparison between the experimentally measured anisotropy and the results of calculations. The used algorithm is based on the inverse distance weighting interpolation method proposed in [10]. The interpolation uses polar coordinates introduced on the (q_{xy}, q_z) plane, which are better adjusted to the geometry of the interpolation problem Q denotes the length of the scattering vector:

$$r \equiv q = \sqrt{q_{xy}^2 + q_z^2} \quad (1)$$

$$\varphi = \text{atan} \left(\frac{q_z}{q_{xy}} \right) \quad (2)$$

A non-typical metric, which was also found to fit the geometry of the interpolation problem well is defined for two points, interpolated point p and data point k as follows, where Δr_{pk} and $\Delta \varphi_{pk}$ are dimensionless radial and angular distances between p and k :

$$\Delta r_{pk} = \frac{r_p - r_k}{0.2[\text{\AA}^{-1}]} \quad (3)$$

$$\Delta \varphi_{pk} = \frac{\varphi_p - \varphi_k}{0.5 \cdot \pi} \quad (4)$$

$$d(p,k) = (\Delta r_{pk})^2 + (\Delta \varphi_{pk})^2 \quad (5)$$

With such a dimensionless metric with defined distance $d(p,k)$, the measured values spread along rings rather than along a scan axis. The weight of the contribution of the intensity at the data point k to the interpolated intensity at point p is:

$$w_k = \frac{1}{[d(p,k)]^3} \quad (6)$$

A final processing method is smoothing the interpolated map 30 times with a smoothing filter with the radius of one pixel to blur sharp edges and removes artifacts in areas where the data point with the highest weight changes rapidly from one interpolation point to another.

Calculations for the model structure

The tentative model of the PANI/CSA crystalline unit cell found by an artificial intelligence optimizer, described in [9], is used as input of the SimDiffraction script for simulating grazing incident beam experiments by D.W. Breiby [11]. Two possible anisotropic film textures described in [8] are used. While polymer chains tend to be oriented in the sample plane, there are two possible preferred crystalline area orientations – one in which the alternating PANI and CSA bilayers tend to be parallel to the film plane, and the other in which bilayer planes tend to be perpendicular to the sample plane. The used software simulates a texture in which several crystalline regions are randomly rotated about an axis perpendicular to the sample plane, with a slight divergence from the above described preferred orientation of bilayer planes versus the sample plane.

RESULTS AND DISCUSSION

All images in this section use a relative intensity scale visualized in grayscale with darker shades corresponding to higher relative intensity value. For clarity however, the shade on the experimental maps does not depend linearly on the intensity, but rather changes rapidly in the low intensity range. This is done to provide higher contrast between peaks and valleys.

Interpolated experimental intensity maps

The intensity map obtained from measurements performed on a PANI/CSA thin film sample cast from *m*-cresol is shown in Fig. 3.

The map shows clear anisotropy of the five main PANI/CSA crystalline peaks. The first and second peaks

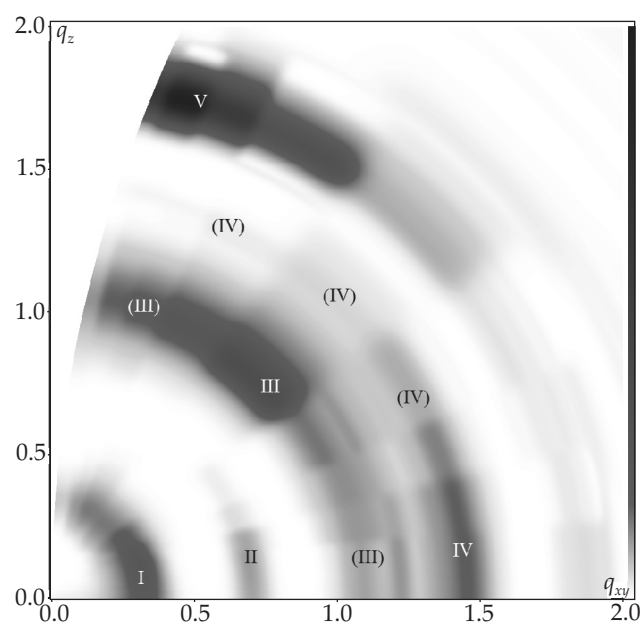


Fig. 3. Interpolated intensity map for a PANI/CSA thin film sample cast from *m*-cresol

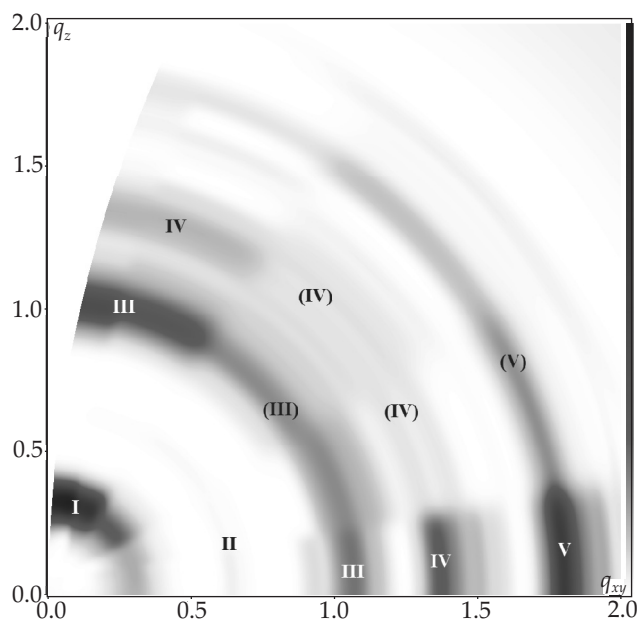


Fig. 4. Interpolated intensity map for a PANI/CSA thin film sample cast from TFA

are oriented in the q_{xy} direction, the fifth in the q_z direction, the third peak has the highest intensity for an intermediate direction, and the fourth peak is slightly more intense in the q_{xy} direction.

The intensity map obtained from measurements performed on a PANI/CSA thin film sample cast from TFA is shown in Fig. 4.

This map shows that the five peaks are anisotropic, but very differently from the previous sample. The second peak is very weak (with its already small intensity decreased in the crystalline component separation algorithm), but clearly present and most intense in the q_{xy} direction. The fourth peak is visible both in the q_{xy} and the q_z directions. The first, third and fifth peaks exhibit an orientation exactly opposite to the previous sample. The first peak is the most intense in the q_z direction, the fifth peak is the most intense in the q_{xy} direction, and the third peak is the least intense for intermediate directions.

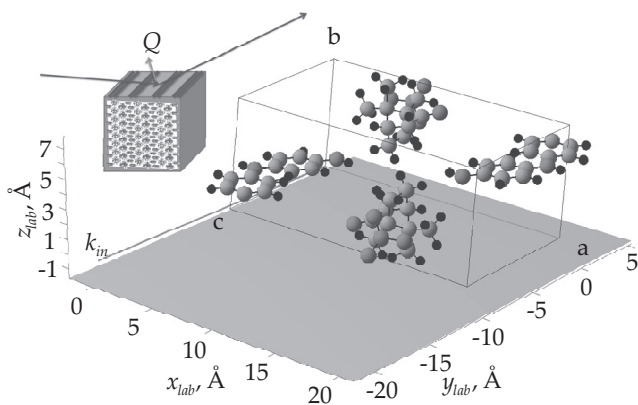


Fig. 5. Orientation of model unit cell relative to the direction of incident beam k_{in} in calculation of intensity map for a PANI/CSA thin film sample cast from *m*-cresol

The above observations lead to a conclusion that the first, second and fifth peaks most probably arise from ordering in three more or less orthogonal directions and the third peak should be a superposition of reflexes of mixed Miller indices, which determine its characteristic anisotropy. The fourth peak does not seem to follow a clear rule and in diffraction patterns registered for bulk samples is much broader than the other peaks, suggesting that it is a superposition of several nearby reflexes, which together do not give it a distinct anisotropy.

Calculated intensity maps

Figure 5 shows the orientation of the model unit cell relative to the direction of the incident beam k_{in} . The z_{lab} direction in calculation corresponds to the out-of-plane direction perpendicular to the film, that is q_z . The bilayer planes orientation in the film is shown in the inset of Fig. 5. The index *lab* in $(x_{lab}, y_{lab}, z_{lab})$ denotes laboratory frame of reference related to crystallite or unit cell orientations in calculations.

There is no preferred orientation of x_{lab} and y_{lab} relative to k_{in} . The in-plane isotropic distribution of crystallites is taken into account in the calculation by averaging rotation of the unit cell around the z_{lab} direction over all q_{xy} orientations. This is depicted in Fig. 6.

For a given diffraction reflex in fully out-of-plane anisotropy one can observe only a single peak, as opposed to a fully isotropic system, which may exhibit a full Debye-Scherrer ring. The experimental intensity map shows partial rings, which means that the system is not perfectly oriented in this direction. To take into account such a behavior, a certain degree of statistical misorientation of crystallites φ_{max} is included in calculations. Comparing intensity maps calculated for different crystallite misorientations with experimental results made it possible to estimate the misorientation angle at about 30 degree, as shown in Fig. 7.

The intensity map calculated in the above described way is shown in Fig. 8. This type of structure is presumed to exist in PANI/CSA thin films cast from *m*-cresol.

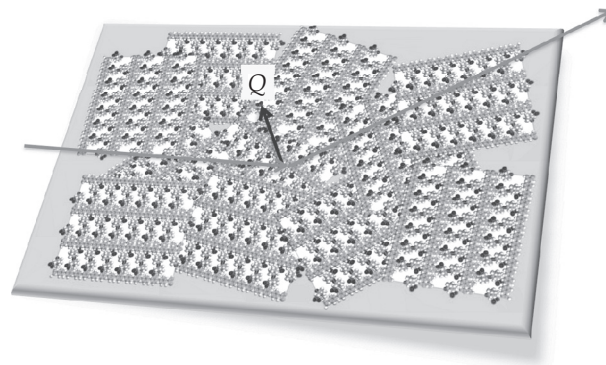


Fig. 6. In-plane isotropic distribution of crystallites on the film surface

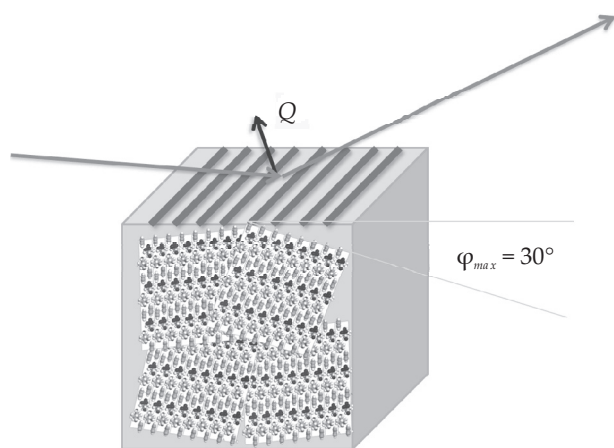


Fig. 7. Out-of-plane statistical misorientation of crystallites included in intensity maps calculations

In the case of this map, the first peak is sharply oriented in the q_{xy} direction. The second peak – which is a composition of mainly the (001) reflex and a weaker (101) reflex, centered at a slightly higher scattering vector value, but overlapping (001) – is also the strongest for this orientation. Several reflexes forming the third peak, with the main ones being (210) and (2-10) followed by the weaker (300), (110), (11-1) and (30-1) give an orientation in intermediate directions, but also a nonzero intensity on the entire ring. The fourth peak, composed of several reflexes, in this case has an intensity tending to zero in the q_z direction, but for other orientations is clearly visible. Finally, the fifth peak, consisting mainly of the (020) reflex with several weak underlying ones has a very sharp orientation in the q_z direction.

All of the above observations made for Fig. 8 are in clear agreement with the statements made for Fig. 3, although

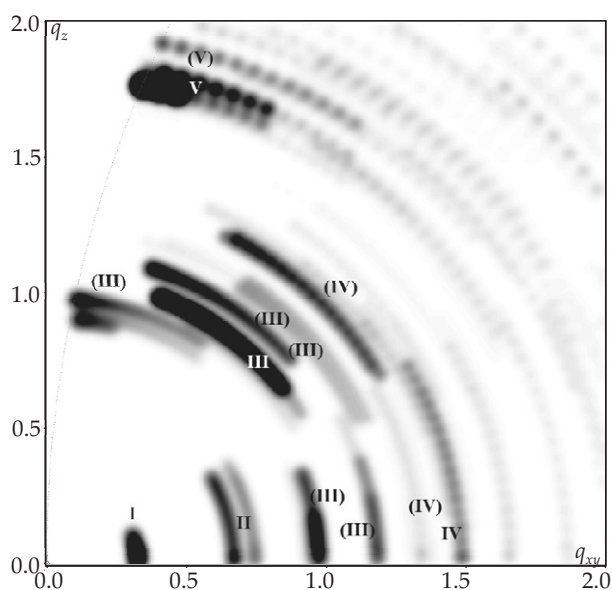


Fig. 8. Calculated intensity map for a PANI/CSA crystalline area distribution with bilayer planes perpendicular to the sample plane (cast from *m*-cresol)

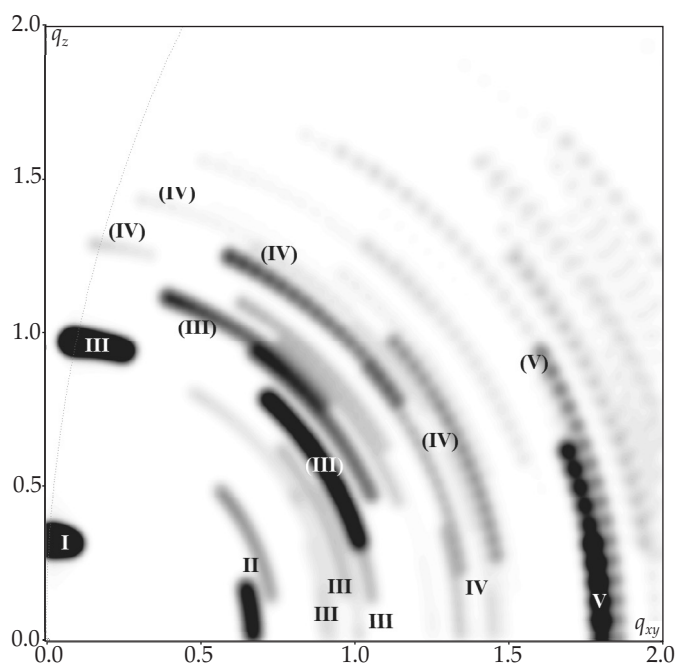


Fig. 9. Calculated intensity map for a PANI/CSA crystalline area distribution with bilayer planes parallel to the sample plane (cast from TFA)

the peaks in the former case are wider in the scattering vector direction Q . This is mainly caused by the smoothing steps of the interpolation process and the ambiguity of the crystalline component extraction procedure.

The second calculated intensity map, for a distribution of crystalline area orientations in which the bilayer planes are mostly parallel to the sample plane, is shown in Fig. 9. This type of structure is presumed to exist in PANI/CSA thin films cast from TFA. The unit cell orientation used in the calculation of this intensity map and bilayers orientation in this case is shown in Fig. 10.

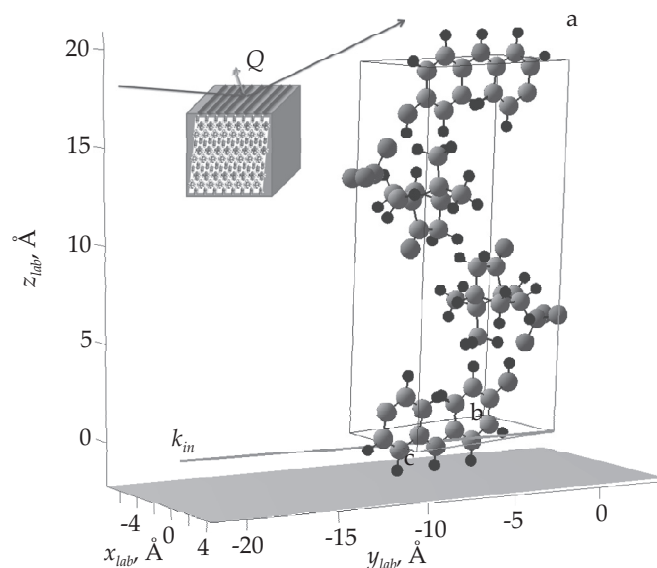


Fig. 10. Orientation of model unit cell relative to the direction of the incident beam k_{in} in calculation of intensity maps for a PANI/CSA thin film sample cast from TFA

The first peak is clearly oriented in the q_z direction, while the second peak prefers the q_{xy} direction, although its intensity is slightly distributed towards the intermediate direction. In the case of the third peak, it is distributed in all orientations, with a higher intensity in the q_z direction, caused by the (300) reflex contribution, and a slight accumulation of reflexes towards the q_{xy} direction. The fourth peak is distributed along the ring and strong statements regarding its anisotropy cannot be made. Finally, the fifth peak strongly prefers the q_{xy} direction.

Comparing the above observations with the ones made when analyzing the anisotropy visible in the extrapolated map in Fig. 4, one can see an agreement also in this case.

CONCLUSIONS

To conclude, two dimensional X-ray surface diffraction intensity maps were calculated by taking advantage of the recently published tentative model of the PANI/CSA crystalline areas published in [9]. To be able to compare these computational results with experimental ones, two dimensional intensity maps were calculated from grazing incident beam diffraction data, after extracting the background and amorphous component and interpolating the intensities outside of the data points.

Such a comparison was performed for samples cast from *m*-cresol, for which it was presumed that bilayer planes are mostly perpendicular to the sample plane, and samples cast from TFA, for which it was presumed that these planes are mostly parallel to the sample plane.

Qualitative remarks concerning the anisotropy of the five main crystalline peak orientations are the same for corresponding pairs of corresponding calculated and experimental maps.

This confirms the statements concerning the agreement of the crystalline area unit cell model with grazing incident beam results from previous papers. This also further validates the indirect statement that PANI/CSA crystalline regions can be described using the same unit cell regardless of the solvent used prior to casting, or – in other words – that solvent molecules are not present in the crystalline regions in an arranged matter.

ACKNOWLEDGMENTS

This work was supported by the Polish Ministry of Science and Higher Education and its grants for Scientific Research.

T. K. would like to thank KNOW – the Marian Smoluchowski Krakow Research Consortium “Matter-Energy-Future” for its support in the form of a scholarship.

D.W. Breiby is acknowledged for suggesting his *SimDiffraction* script.

REFERENCES

- [1] Epstein A.J., Ginder J.M., Zuo F. *et al.*: *Synthetic Metals* **1987**, *21*, 63.
[http://dx.doi.org/10.1016/0379-6779\(87\)90067-1](http://dx.doi.org/10.1016/0379-6779(87)90067-1)
- [2] Zhou Y., Wang Y., He D. *et al.*: *Journal of Nanoscience and Nanotechnology* **2014**, *14*, 3417.
<http://dx.doi.org/10.1166/jnn.2014.7959>
- [3] Anno H., Hokazono M., Akagi F. *et al.*: *Journal of Electronic Materials* **2013**, *42*, 1346.
<http://dx.doi.org/10.1007/s11664-012-2368-z>
- [4] Pang Z., Fu J., Lv P. *et al.*: *Sensors* **2014**, *14*, 21 453.
<http://dx.doi.org/10.3390/s141121453>
- [5] Łużny W., Samuelsen E.J., Breiby D.W.: *Synthetic Metals* **2001**, *119*, 203.
[http://dx.doi.org/10.1016/S0379-6779\(00\)00736-0](http://dx.doi.org/10.1016/S0379-6779(00)00736-0)
- [6] Łużny W., Samuelsen E.J., Breiby D.W.: *Fibres & Textiles in Eastern Europe* **2003**, *11*, 97.
- [7] Śniechowski M., Borek R., Piwowarczyk K., Łużny W.: *Macromolecular Theory and Simulations* **2015**, *24*, 284. <http://dx.doi.org/10.1002/mats.201400105>
- [8] Śniechowski M., Kozik T., Niedźwiedź W., Łużny W.: *Macromolecular Theory and Simulations* **2016**, *25*, 328.
<http://dx.doi.org/10.1002/mats.201600010>
- [9] Kozik T., Śniechowski M., Łużny W. *et al.*: *Polymer* **2017**, *111*, 148.
<http://dx.doi.org/10.1016/j.polymer.2017.01.034>
- [10] Shepard D.: “A two-dimensional interpolation function for irregularly-spaced data”, Proceedings of the 1968 23rd ACM national conference, New York, USA, August 27–29, 1968, 517.
<http://dx.doi.org/10.1145/800186.810616>
- [11] Breiby D.W., Bunk O., Andreasen J.W. *et al.*: *Journal of Applied Crystallography* **2008**, *41*, 262.
<http://dx.doi.org/10.1107/S0021889808001064>

Received 7 IV 2017.